Mean and variance of the forward field propagated through three-dimensional random internal waves in a continental-shelf waveguide

Tianrun Chen
Department of Mechanical Engineering, Massachusetts Institute of Technology, Cambridge, Massachusetts 02139

Purnima Ratilal
Department of Electrical and Computer Engineering, Northeastern University, Boston, Massachusetts 02115

Nicholas C. Makris
Department of Mechanical Engineering, Massachusetts Institute of Technology, Cambridge, Massachusetts 02139

(Received 30 May 2004; revised 3 June 2005; accepted 12 June 2005)

The mean and variance of the acoustic field forward propagated through a stratified ocean waveguide containing three-dimensional (3-D) random internal waves is modeled using an analytic normal mode formulation. The formulation accounts for the accumulated effects of *multiple forward scattering*. These lead to redistribution of both coherent and incoherent modal energies, including attenuation and dispersion. The inhomogeneous medium's scatter function density is modeled using the Rayleigh-Born approximation to Green's theorem to account for random fluctuations in both density and compressibility caused by internal waves. The generalized waveguide extinction theorem is applied to determine attenuation due to scattering from internal wave inhomogeneities. Simulations for typical continental-shelf environments show that when internal wave height exceeds the acoustic wavelength, the acoustic field becomes so randomized that the expected total intensity is dominated by the field variance beyond moderate ranges. This leads to an effectively saturated field that decays monotonically and no longer exhibits the periodic range-dependent modal interference structure present in nonrandom waveguides. Three-dimensional scattering effects can become important when the Fresnel width approaches and exceeds the cross-range coherence length of the internal wave field. Density fluctuations caused by internal waves are found to noticably affect acoustic transmission in certain Arctic environments. [DOI: 10.1121/1.1993107]

PACS number(s): 43.30.Re [WLS] Pages: 3560–3574

I. INTRODUCTION

When an acoustic field propagates through a multimodal waveguide, random variations in medium properties can have a cumulative effect over range. This can drastically alter the delicate modal interference structure of the incident field, leading to significant randomization in the received field. Here, we model the mean, variance, and total intensity of the forward field propagated through an ocean waveguide containing temporally and spatially random 3-D internal waves using a general modal formulation described in Ref. 1. This formulation is convenient because it takes into account the accumulated effects of *multiple forward scattering* on the *mean and covariance* of the forward propagated field. These include coherent, partially coherent, and incoherent interactions with the incident field, which lead to attenuation, dispersion, and exponential coefficients of field variance that describe mode coupling induced by the medium's inhomogeneities. An advantage of the formulation is that the first and second moments of the forward field can be analytically expressed in terms of the first and second moments of the inhomogeneous medium's spatially varying scatter function density. These inhomogeneities can be arbitrarily large relative to the acoustic wavelength and have arbitrary compressibility and density contrast from the surrounding medium.

Inhomogeneities arising from internal wave disturbances typically have relatively small differences in density and compressibility from the surrounding medium. A convenient approach for modeling their scattering properties is to apply the first-order Rayleigh-Born approximation to Green's theorem.[2] Internal wave scattering properties are then expressed in terms of the statistical variations in compressibility and density caused by the disturbance. This requires knowledge of the probability distributions of the compressibility and density variations, which can be expressed in terms of internal-wave wave number spectra. The first-order Rayleigh-Born approximation leads to a purely real scatter function that can directly account for scattering-induced dispersion in the mean forward field, but not attenuation, which requires the imaginary part. Attenuation in the mean forward field due to scattering is then determined from the waveguide extinction theorem.[3,4] The waveguide extinction theorem for any given mode relates power loss in the *forward* azimuth to

the total scattered power in all directions, which can be estimated with high accuracy using the first-order Rayleigh-Born approximation.

Following the trend of ever-increasing ocean utilization has come a greater interest in developing models to help understand and accurately predict the effect of internal wave fields on underwater acoustic transmission through continental shelf environments. Significant fluctuations have been observed[5–7] and predicted[8,9] in signal transmission. These fluctuations lead to signal-dependent noise[8] that can significantly degrade sonar system performance. Since internal waves in continental shelf environments often have large displacements compared to the acoustic wavelength and large slopes, standard perturbation theory methods for modeling the effect of rough surface scattering[10–13] on acoustic transmission through an ocean waveguide may often be unsuitable. If the accumulated effects of multiple forward scattering on dispersion and field variance are important in acoustic propagation through extended internal wave fields, approaches that neglect them[10–13] may be inappropriate, as noted in Ref. 14. It is possible that acoustic transmission through such complicated environments may be seriously altered by three-dimensional (3-D) scattering effects beyond relatively short ranges. Two-dimensional models,[6,13,15–17] 2-D Monte-Carlo simulations,[18] and adiabatic 3-D models[19] may then also become unreliable.

The present formulation is advantageous because the mean and variance of the acoustic field multiply forward scattered through a 3-D random waveguide can be rapidly obtained from the compact analytic expressions of Ref. 1, given the mean and spatial covariance of the internal wave displacement field, without restriction on internal wave amplitude or slope. It can be readily applied to solve a variety of underwater remote sensing and communication problems in continental shelf environments. This includes the detection and localization of sources[20,21] and targets by passive and active sonar, as well as the estimation of biological,[22,23] geological,[24] and oceanographic parameters[25] by seismoacoustic inverse methods.

We show that the accumulated effect of multiple forward scattering through random internal wave fields typically must be included to properly model the statistical moments of the acoustic field forward propagated through continental shelf environments. We also show that 3-D multiple scattering effects can become important in both the mean and variance of the forward field. This is because, as the source-receiver range increases, the Fresnel width of the forward field eventually exceeds the cross-range coherence length of the internal waves, making out-of-plane scattering important when internal wave amplitudes exceed the acoustic wavelength and slopes become higher. Out-of-plane scattering cannot be accounted for in 2-D models. We illustrate this effect by comparing the present 3-D model with a current standard approach, which is to compute field moments by Monte-Carlo simulations with the 2-D parabolic equation.

We show that the acoustic field moments are highly dependent on both the rms displacements and coherence scales of the 3-D internal waves. In a waveguide where the rms internal wave height is small compared to the acoustic wavelength, the forward field remains coherent and exhibits the range and depth-dependent structure expected from the coherent interference between waveguide modes. The moderate dispersion and attenuation induced by multiple forward scatter through the internal wave disturbances still noticeably alters the mean field. Scattering in such a slightly random waveguide may not be strong enough to make 3-D effects noticable.

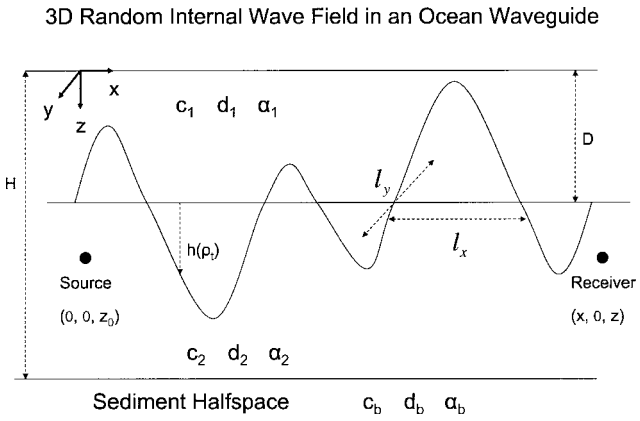

FIG. 1. Geometry of mid-latitude Atlantic continental shelf and Arctic environments with two-layer water column of total depth $H_w = 100$ m, and upper layer depth of $D = 30$ m. The bottom sediment half-space is composed of sand. The internal wave disturbances have coherence length scales l_x and l_y in the x and y directions, respectively, and are measured with positive height h measured downward from the interface between the upper and lower water layers.

When the rms internal wave height becomes larger than the acoustic wavelength, 3-D scattering effects become significant. The field variance or incoherent intensity is found to dominate the total intensity of the forward field beyond moderate propagation ranges. This causes the acoustic field to become fully saturated. In this case, the coherent modal interference structure in range and depth is lost, and the intensity of the forward field then decays monotonically. This makes standard processing techniques that rely upon model coherence, such as matched field processing and the waveguide-invariant method[26] for source range and depth localization, far less effective.

The effects on acoustic transmission of random density fluctations in the medium due to internal waves are also quantified. We show that internal-wave-induced density effects can significantly affect acoustic propagation in specific environments, such as Arctic seas.

II. FORMULATION IN A TWO-LAYER WATER COLUMN

Internal waves in mid-latitude continental shelf environments often occur at the interface between warm water near the sea surface and cooler water below.[7,27,28] In high latitude, the reverse is usually true where the cooler less dense water above comes from recently melted ice. Here, we model the internal wave field as disturbances propagating along the boundary between strata in a two-layer water-column, as illustrated in Fig. 1. Although many other internal wave models and parametrizations could have been used to implement the general formulation of Ref. 1, the two-layer model is chosen here because it clearly illustrates the fundamental

physics of internal waves in a continental shelf environment. This has made it probably the most frequently used model in the literature.[29–31] We focus on the baroclinic mode of the internal wave, which has negligible displacement at the sea surface.[30] In the absence of internal waves, the boundary separating the upper medium with density d_1 and sound speed c_1 from the lower medium with density d_2 and sound speed c_2 is at a constant depth. In the presence of internal waves, a part of the lower medium protrudes into the upper medium and a part of the upper medium protrudes into the lower medium. We model protrusion of the lower medium into the upper medium as a volumetric inhomogeneity that scatters the sound field by Green's theorem, and *vice versa* for the lower medium.

To formulate the problem, we place the origin of the coordinate system at the sea surface. The z axis points downward and normal to the interface between horizontal strata. The water depth is H and the boundary separating the upper and lower medium is at depth $z=D$. Let coordinates of the source be defined by $\mathbf{r}_0=(0,0,z_0)$, and receiver coordinates by $\mathbf{r}=(x,0,z)$. Spatial cylindrical (ρ,ϕ,z) and spherical systems (r,θ,ϕ) are defined by $x=r\sin\theta\cos\phi$, $y=r\sin\theta\sin\phi$, $z=r\cos\theta$, and $\rho=x^2+y^2$. The horizontal and vertical wave number components for the nth mode are, respectively, $\xi_n=k\sin\alpha_n$ and $\gamma_n=k\cos\alpha_n$, where α_n is the elevation angle of the mode measured from the z axis. Here, $0\leqslant\alpha_n\leqslant\pi/2$ so that the down- and upgoing plane wave components of each mode will then have elevation angles α_n and $\pi-\alpha_n$, respectively. The corresponding vertical wave number of the down- and upgoing components of the nth mode are γ_n and $-\gamma_n$, respectively, where $\Re\{\gamma_n\}\geqslant 0$. The wave number magnitude k equals the angular frequency ω divided by the sound speed c in the object layer so that $k^2=\xi_n^2+\gamma_n^2$. The azimuth angle of the modal plane wave is denoted by β, where $0\leqslant\beta\leqslant 2\pi$. The geometry of spatial and wave number coordinates is shown in Ref. 32.

A. Statistical description of internal waves

1. Joint spatial probability density of internal wave displacement

The displacement $h(\boldsymbol{\rho}_t)$ of the internal wave boundary at horizontal location $\boldsymbol{\rho}_t$, as illustrated in Fig. 1, can be modeled as a Gaussian random process in space and time with mean $\langle h\rangle$, and variance $\eta_h^2=\langle h^2\rangle-\langle h\rangle^2$. Since the baroclinic internal wave displacement cannot penetrate the water surface or the sea bottom, we limit unphysical tails of the probability density function by windowing h. The probability density function of the internal wave displacement is,

$$p_h(h)=\begin{cases} T\dfrac{1}{\sqrt{2\pi}\eta_h}\mathrm{e}^{-(h-\langle h\rangle)^2/2\eta_h^2}, & \text{for } \langle h\rangle-h_1\leqslant h\leqslant\langle h\rangle+h_2,\\ 0 \quad \text{elsewhere}, \end{cases} \tag{1}$$

where $T=1/[P((\langle h\rangle+h_2)/\eta_h)-P((\langle h\rangle-h_1)/\eta_h)]$ is a normalization constant, and $P(b)$ is the cumulative distribution function,

$$P(b)=\frac{1}{\sqrt{2\pi}}\int_{-\infty}^{b}\mathrm{e}^{-m^2/2}\,dm. \tag{2}$$

Linear internal wave displacements are expected to follow a zero-mean circular complex Gaussian random process by the central limit theorem, given that they arise from the superposition of many statistically independent sources in space and time. The same model can also be used to describe nonlinear solitary internal waves in some cases when they are incompletely evolved[33] or broadly distributed in peak amplitude.[34] For nonlinear internal wave fields, nonzero mean displacements and much larger standard deviations are expected.

The joint probability density function of the internal wave displacement at horizontal locations $\boldsymbol{\rho}_t$ and $\boldsymbol{\rho}_t'$ can be expressed as

$$p(h(\boldsymbol{\rho}_t),h(\boldsymbol{\rho}_t'))=\frac{1}{2\pi\eta_{h(\boldsymbol{\rho}_t)}\eta_{h(\boldsymbol{\rho}_t')}(1-\varrho^2)^{1/2}}\exp\left(-\frac{[(h^2(\boldsymbol{\rho}_t)\eta^2_{h(\boldsymbol{\rho}_t')}-2h(\boldsymbol{\rho}_t)h(\boldsymbol{\rho}_t')\varrho\,\eta_{h(\boldsymbol{\rho}_t)}\eta_{h(\boldsymbol{\rho}_t')}+h^2(\boldsymbol{\rho}_t')\eta^2_{h(\boldsymbol{\rho}_t)})]}{2\eta^2_{h(\boldsymbol{\rho}_t)}\eta^2_{h(\boldsymbol{\rho}_t')}(1-\varrho^2)}\right), \tag{3}$$

where ϱ is the correlation coefficient defined as

$$\varrho=\frac{\langle h(\boldsymbol{\rho}_t)h(\boldsymbol{\rho}_t')\rangle-\langle h(\boldsymbol{\rho}_t)\rangle\langle h(\boldsymbol{\rho}_t')\rangle}{\sqrt{(\langle|h(\boldsymbol{\rho}_t)|^2\rangle-|\langle h(\boldsymbol{\rho}_t)\rangle|^2)(\langle|h(\boldsymbol{\rho}_t')|^2\rangle-|\langle h(\boldsymbol{\rho}_t')\rangle|^2)}}. \tag{4}$$

2. Linear internal wave field as a stationary random process

For random internal wave fields that follow a stationary random process in space, the internal wave displacement correlation function and standard deviation η_h can be expressed in terms of the internal wave spectrum $\mathcal{G}(\boldsymbol{\kappa})$. For instance, the correlation function is

$$\langle h(\boldsymbol{\rho}_t)h(\boldsymbol{\rho}_t')\rangle=C_{hh}(\boldsymbol{\rho}_t-\boldsymbol{\rho}_t')=\frac{1}{(2\pi)^2}\int_0^{2\pi}\int_0^{\infty}\mathcal{G}(\boldsymbol{\kappa})e^{i\boldsymbol{\kappa}\cdot(\boldsymbol{\rho}_t-\boldsymbol{\rho}_t')}\kappa\,\mathrm{d}\kappa\,\mathrm{d}\Theta, \tag{5}$$

where $\boldsymbol{\kappa}=(\kappa_x,\kappa_y)=(\kappa\cos\Theta,\kappa\sin\Theta)$ is the internal-wave wave number vector with magnitude κ and azimuthal di-

rection Θ. The internal wave height standard deviation η_h is defined by

$$\eta_h^2 = C_{hh}(0), \tag{6}$$

when $\langle h \rangle = 0$, as is the case for linear internal waves.

The internal wave disturbance has a horizontal coherence area given by[35]

$$A_c = \frac{\int_0^{2\pi}\int_0^{\infty} |C_{hh}(\rho,\Theta)|^2 \rho \, d\rho \, d\Theta}{|C_{hh}(0)|^2}, \tag{7}$$

where $\boldsymbol{\rho} = \boldsymbol{\rho}_t - \boldsymbol{\rho}_t' = \rho \cos\Theta \mathbf{x} + \rho \sin\Theta \mathbf{y}$, outside of which internal wave displacements can be assumed to be uncorrelated.[1] The corresponding coherence length scale of the internal wave disturbance $l_c(\Theta)$ in any azimuthal direction Θ is then given by

$$l_c^2(\Theta) = \frac{2\int_0^{\infty} |C_{hh}(\rho,\Theta)|^2 \rho \, d\rho}{|C_{hh}(0)|^2}. \tag{8}$$

Here $l_c(\Theta)$ defines a coherence shape function for the internal wave disturbance that is determined as its wave number spectrum spans the 2π azimuthal radians of Θ. The full coherence lengths l_x and l_y of the internal wave disturbance in the x and y directions are then, respectively,

$$l_x = l_c(\Theta = 0) + l_c(\Theta = \pi) \tag{9}$$

and

$$l_y = l_c(\Theta = \pi/2) + l_c(\Theta = 3\pi/2). \tag{10}$$

For an isotropic internal wave field, Eq. (5) reduces to

$$C_{hh}(\boldsymbol{\rho}_t - \boldsymbol{\rho}_t') = \frac{1}{2\pi}\int_0^{\infty} \mathcal{G}(\kappa) J_0(\kappa|\boldsymbol{\rho}_t - \boldsymbol{\rho}_t'|) \kappa \, d\kappa, \tag{11}$$

since its wave number spectrum $\mathcal{G}(\kappa)$ is independent of the azimuth angle Θ.

B. Scatter function of an internal wave inhomogeneity

To determine the plane wave scatter function of a coherence volume of internal wave inhomogeneity, we apply Green's theorem,[2]

$$\Phi_s(\mathbf{r}|\mathbf{r_0}) = \iiint [k^2 \Gamma_\kappa(\mathbf{r_t}) \Phi(\mathbf{r_t}|\mathbf{r_0}) G(\mathbf{r}|\mathbf{r}_t) + \Gamma_d(\mathbf{r_t}) \boldsymbol{\nabla} \Phi(\mathbf{r_t}|\mathbf{r_0}) \cdot \boldsymbol{\nabla} G(\mathbf{r}|\mathbf{r_t})] dV_t, \tag{12}$$

where Γ_κ is the fractional change in compressibility and Γ_d is the fractional change in density of the inhomogeneity centered at $\mathbf{r}_t$ relative to the original medium, $G(\mathbf{r}|\mathbf{r_t})$ is the free space Green's function, and $\Phi(\mathbf{r_t}|\mathbf{r_0})$ is the total acoustic field in the volume of inhomogeneity. To integrate Eq. (12) analytically, we need to know the total field within the volume of the inhomogeneity. But this is the sum of the known incident and unknown scattered field in the volume. In the first-order Rayleigh-Born approximation, the total field inside the inhomogeneity is approximated by the incident field. This is a good approximation when the scattered field within the inhomogeneity is small compared to the incident field as it typically is when the fractional compressibility and density changes are small, as they are in the present scenario. Green's theorem evaluated using the first-order Rayleigh-Born approximation then provides a first-order estimate of the scattered field from an inhomogeneity. From this we can obtain a first-order estimate of the inhomogeneity's plane wave scatter function.

We first derive the plane wave scatter function for a coherent volume of internal wave inhomogeneity centered at horizontal location $\boldsymbol{\rho}_s$, where $\boldsymbol{\rho}_t = \boldsymbol{\rho}_s + \mathbf{u}_t$. For an incoming plane wave in the direction $\mathbf{k}_i = (k, \alpha_i, \beta_i) = (\boldsymbol{\xi}_i, \gamma_i)$ and scattered plane wave in the direction $\mathbf{k} = (k, \alpha, \beta) = (\boldsymbol{\xi}, \gamma)$, the first-order scatter function of an internal wave inhomogeneity is

$$\Re\{S_{\boldsymbol{\rho}_s}(\alpha,\beta,\alpha_i,\beta_i)\} = \iint_{A_c}\int_0^H \frac{k^3}{4\pi}[\Gamma_\kappa(\mathbf{r}_t) + \eta(\mathbf{k},\mathbf{k}_i)\Gamma_d(\mathbf{r}_t)] \times e^{i[(\boldsymbol{\xi}_i - \boldsymbol{\xi})\cdot\mathbf{u}_t + (\gamma_i - \gamma)z_t]} d^2\mathbf{u}_t \, dz_t, \tag{13}$$

by application of Green's theorem, Eq. (12), where

$$\eta(\mathbf{k},\mathbf{k}_i) = (\mathbf{k}_i \cdot \mathbf{k})/k^2 = \cos\alpha_i \cos\alpha + \sin\alpha_i \sin\alpha \cos(\beta_i - \beta) \tag{14}$$

is the cosine of the angle between the incident and scattered plane wave directions. The fractional changes in compressibility and density depend on the displacement of the inhomogeneities at $\mathbf{r_t}$ and are given by

$$\Gamma_\kappa(\mathbf{r}_t) = \Gamma_\kappa(h(\boldsymbol{\rho}_t), z_t) = \frac{\kappa_1 - \kappa_2}{\kappa_2} U[h(\boldsymbol{\rho}_t) - (z_t - D)] U(z_t - D) + \frac{\kappa_2 - \kappa_1}{\kappa_1} U[(z_t - D) - h(\boldsymbol{\rho}_t)] U(-(z_t - D)), \tag{15}$$

and

$$\Gamma_d(\mathbf{r}_t) = \Gamma_d(h(\boldsymbol{\rho}_t), z_t) = \frac{d_1 - d_2}{d_1} U[h(\boldsymbol{\rho}_t) - (z_t - D)] U(z_t - D) + \frac{d_2 - d_1}{d_2} U[(z_t - D) - h(\boldsymbol{\rho}_t)] U(-(z_t - D)), \tag{16}$$

where U is the unit step function.

The areal scatter function density $s_{\boldsymbol{\rho}_s, z_t}(\alpha,\beta,\alpha_i,\beta_i)$ centered at $(\boldsymbol{\rho}_s, z_t)$ is related to the scatter function $S_{\boldsymbol{\rho}_s}(\alpha,\beta,\alpha_i,\beta_i)$ of Eq. (13) by

$$S_{\boldsymbol{\rho}_s}(\alpha,\beta,\alpha_i,\beta_i) = A_c \int_0^H s_{\boldsymbol{\rho}_s, z_t}(\alpha,\beta,\alpha_i,\beta_i) e^{i(\gamma_i - \gamma)z_t} \, dz_t, \tag{17}$$

where

$$s_{\boldsymbol{\rho}_s, z_t}(\alpha,\beta,\alpha_i,\beta_i) = \frac{1}{A_c}\iint_{A_c} \frac{k^3}{4\pi}[\Gamma_\kappa(\mathbf{r}_t) + \eta(\mathbf{k},\mathbf{k}_i)\Gamma_d(\mathbf{r}_t)] e^{i(\boldsymbol{\xi}_i - \boldsymbol{\xi})\cdot\mathbf{u}_t} \, d^2\mathbf{u}_t. \tag{18}$$

1. Mean and correlation function of the scatter function density of internal wave inhomogeneities

The scatter function density $s_{\boldsymbol{\rho}_s,z_t}(\alpha,\beta,\alpha_i,\beta_i)$ of Eq. (18) is a random variable since it depends on the internal wave displacement $h(\boldsymbol{\rho}_t)$. The mean of the scatter function density is

$$\langle s_{\boldsymbol{\rho}_s,z_t}(\alpha,\beta,\alpha_i,\beta_i)\rangle = \frac{1}{A_c}\iint_{A_c}\left[\int \frac{k^3}{4\pi}[\Gamma_\kappa(h(\boldsymbol{\rho}_t),z_t)+\eta(\mathbf{k},\mathbf{k}_i)\Gamma_d(h(\boldsymbol{\rho}_t),z_t)]p_h(h)\mathrm{d}h\right]e^{i(\boldsymbol{\xi}_i-\boldsymbol{\xi})\cdot\mathbf{u_t}}\,\mathrm{d}^2\mathbf{u_t}$$
$$= \frac{1}{A_c}\left\langle \frac{k^3}{4\pi}[\Gamma_\kappa(h(\boldsymbol{\rho}_t),z_t)+\eta(\mathbf{k},\mathbf{k}_i)\Gamma_d(h(\boldsymbol{\rho}_t),z_t)]\right\rangle \iint_{A_c} e^{i(\boldsymbol{\xi}_i-\boldsymbol{\xi})\cdot\mathbf{u_t}}\,\mathrm{d}^2\mathbf{u_t}. \tag{19}$$

For two inhomogeneities centered at $(\boldsymbol{\rho}_s,z_t)$ and $(\boldsymbol{\rho}_s',z_t')$, respectively, the correlation of their scatter function densities is

$$\langle s_{\boldsymbol{\rho}_s,z_t}(\alpha,\beta,\alpha_i,\beta_i)s^*_{\boldsymbol{\rho}_s',z_t'}(\alpha',\beta',\alpha_i',\beta_i')\rangle = \left(\frac{1}{A_c}\right)^2\iint_{A_c}\iint_{A_c'} e^{i[(\boldsymbol{\xi}_i-\boldsymbol{\xi})\cdot\boldsymbol{\rho}_t-(\boldsymbol{\xi}_i'-\boldsymbol{\xi}')\cdot\boldsymbol{\rho}_t']}C_{\mathcal{FF}}(\boldsymbol{\rho}_t-\boldsymbol{\rho}_t',z_t,z_t')\mathrm{d}^2\mathbf{u}_t\,\mathrm{d}^2\mathbf{u}_t', \tag{20}$$

where

$$C_{\mathcal{FF}}(\boldsymbol{\rho}_t-\boldsymbol{\rho}_t',z_t,z_t')$$
$$= \iint\left(\frac{k^3}{4\pi}\right)^2[\Gamma_\kappa(h(\boldsymbol{\rho}_t),z_t)+\eta(\mathbf{k},\mathbf{k}_i)\Gamma_d(h(\boldsymbol{\rho}_t),z_t)][\Gamma_\kappa(h(\boldsymbol{\rho}_t'),z_t')+\eta(\mathbf{k}',\mathbf{k}_i')\Gamma_d(h(\boldsymbol{\rho}_t'),z_t')]p(h(\boldsymbol{\rho}_t),h(\boldsymbol{\rho}_t'))\mathrm{d}h(\boldsymbol{\rho}_t)\mathrm{d}h(\boldsymbol{\rho}_t'), \tag{21}$$

following the notation of Ref. 1, Appendix A.

The joint probability function $p(h(\boldsymbol{\rho}_t),h(\boldsymbol{\rho}_{t'}))$ requires the internal wave spectrum to be specified, as can be seen from Eqs. (3)–(5).

2. Isotropic internal waves

We must calculate the mean and spatial covariance of the scatter function density $s_{\boldsymbol{\rho}_s,z_t}(\alpha,\beta,\alpha_i,\beta_i)$ to determine the forward field moments. This requires the internal wave spectrum defined in Eq. (5) to be specified. Following Refs. 18 and 6, we assume the internal waves follow the isotropic Garret-Munk spectrum,

$$\mathcal{G}(\boldsymbol{\kappa}) = E_0\frac{2}{\pi^2}\frac{\omega_c\sqrt{\kappa^2c_g^2-\omega_c^2}}{\kappa^4c_g^2}, \tag{22}$$

for the relatively high wave numbers of interest in our analysis, where E_0 is the average energy density that determines the strength of the internal wave fluctuation, ω_c is the Coriolis frequency, which is roughly 1.16×10^{-5} Hz at 30° lattitude, and $c_g\approx0.4$ m/s is the phase speed of the internal waves in the two-layer ocean, given by $c_g^2=g[(\rho_2-\rho_1)/\rho_2][D(H-D)/H]$, where g is the gravitational acceleration. The corresponding coherence radius $l_c(\theta_t)=l_c$ is then independent of azimuth.

In this paper, we focus our analysis on internal wave fluctuations that occur within a measurement time scale T. Within this time, only internal wave disturbances that occur with frequencies that are larger than $f_{\min}=1/T$ or equivalently have wave numbers larger than $\kappa_{\min}=2\pi f_{\min}/c_g=2\pi/c_gT$ can cause temporal fluctuation in the acoustic field. From Eq. (22), Eq. (8) and Eq. (7), the coherence radius is then $l_c=\sqrt{2}/\kappa_{\min}$, the x and y coherence lengths are $l_x=l_y=2\sqrt{2}/\kappa_{\min}$, and the coherence area is $A_c=\pi l_c^2=2\pi/\kappa_{\min}^2$.

As noted in Ref. 1, the cross-range coherence length l_y of internal wave inhomogeneities can be greater or less than the Fresnel width $Y_{\mathrm{F}}(\rho,\rho_s)\approx\sqrt{\lambda(\rho-\rho_s)\rho_s/\rho}$, which depends on the range ρ from source to receiver and the range ρ_s from source to the inhomogeneities. When $l_y<Y_{\mathrm{F}}$, decorrelation in the cross-range occurs within the Fresnel width or active region. But when $l_y>Y_{\mathrm{F}}$, internal wave inhomogeneities are fully correlated across the active region. In this case, only the portion of the coherence area A_{F} within the Fresnel width is important to forward scatter, where $A_{\mathrm{F}}\leqslant A_c$.

C. Statistical moments of the forward propagated field

The mean field, variance, and expected total intensity of the forward field propagated through the ocean waveguide containing random internal waves can be expressed analytically using the formulation of Ref. 1. We assume that the internal wave inhomogeneities obey a stationary random process in range. For a source at $\mathbf{r_0}=(0,0,z_0)$ and a receiver at $\mathbf{r}=(x,0,z)$, the mean forward field is given by Eq. (83) of Ref. 1 as

$$\langle\Psi_T(\mathbf{r}|\mathbf{r_0})\rangle = \sum_n \Psi_i^{(n)}(\mathbf{r}|\mathbf{r_0})\mathrm{e}^{i\int_0^\rho\nu_n(\rho_s)\mathrm{d}\rho_s}, \tag{23}$$

where

$$\Psi_i^{(n)}(\mathbf{r}|\mathbf{r_0}) = 4\pi\frac{i}{d(z_0)\sqrt{8\pi}}\mathrm{e}^{-i\pi/4}u_n(z)u_n(z_0)\frac{\mathrm{e}^{i\xi_n\rho}}{\sqrt{\xi_n\rho}} \tag{24}$$

is the incident field contribution from mode n, given no inhomogeneities in the medium, $u_n(z)$ is the modal amplitude at depth z, and ν_n is the horizontal wave number change due to multiple scattering from the inhomogeneities. The modal horizontal wave number change is complex, and it leads to both dispersion and attenuation in the mean forward field.

The real part $\Re\{\nu_n\}$ is the modal dispersion coefficient and the imaginary part $\Im\{\nu_n\}$ is the modal attenuation coefficient.

For the present case, where the random inhomogeneities are due to internal waves,

$$\int_0^\rho \nu_n(\rho_s)\mathrm{d}\rho_s = \int_0^\rho \frac{1}{\xi_n}\langle \Xi_h(n,n,0,0)\rangle \mathrm{d}\rho_s, \tag{25}$$

from Eq. (60) of Ref. 1, where

$$\begin{aligned}\Xi_h(m,n,\beta,\beta_i) &= \int_0^H \frac{2\pi}{k(z_t)d(z_t)}[N_m^{(1)}N_n^{(1)}\mathrm{e}^{i\Re\{\gamma_m+\gamma_n\}z_t}s_{\rho_s,z_t}(\pi-\alpha_m,\beta;\alpha_n,\beta_i) \\ &\quad - N_m^{(2)}N_n^{(1)}\mathrm{e}^{i\Re\{-\gamma_m+\gamma_n\}z_t}s_{\rho_s,z_t}(\alpha_m,\beta;\alpha_n,\beta_i) \\ &\quad - N_m^{(1)}N_n^{(2)}\mathrm{e}^{i\Re\{\gamma_m-\gamma_n\}z_t}s_{\rho_s,z_t}(\pi-\alpha_m,\beta;\pi-\alpha_n,\beta_i) \\ &\quad + N_m^{(2)}N_n^{(2)}\mathrm{e}^{i\Re\{-\gamma_m-\gamma_n\}z_t}s_{\rho_s,z_t}(\alpha_m,\beta;\pi-\alpha_n,\beta_i)] \\ &\quad \times \mathrm{e}^{-\Im\{\gamma_m+\gamma_n\}z_t}\,\mathrm{d}z_t.\end{aligned} \tag{26}$$

As discussed in Sec. II B, substituting Eq. (18) into Eq. (25) leads to a modal horizontal wave number change that is purely real. This accounts for the dispersion, but not the attenuation in the mean forward field due to scattering. The modal attenuation coefficients $\Im\{\nu_m\}$ will be derived in Sec. II D from the waveguide extinction theorem.[3]

From Eq. (25), we see that the modal dispersion coefficients depend on the expected scatter function density in the forward azimuth. This is independent of the cross-range extent of the internal wave inhomogeneities, so the dispersion coefficients are also range independent.

The variance of the forward field at the receiver can be expressed by Eq. (84) of Ref. 1 as

$$\begin{aligned}\mathrm{Var}(\Psi_T(\mathbf{r}|\mathbf{r_0})) = \sum_n \frac{2\pi}{d^2(z_0)}\frac{1}{|\xi_n|\rho}|u_n(z_0)|^2|u_n(z)|^2 \\ \times \mathrm{e}^{-2\Im\left\{\xi_n\rho+\int_0^\rho \nu_n(\rho_s)\mathrm{d}\rho_s\right\}}\left(\mathrm{e}^{\int_0^\rho \mu_n(\rho_s)\mathrm{d}\rho_s}-1\right),\end{aligned} \tag{27}$$

where μ_n is defined in Ref. 1 as the exponential coefficient of modal field variance. The variance of the forward field depends on the first- and second-order moments of the scatter function density of the random medium. An analytic expression for μ_n for general surface and volume inhomogeneities is provided in Ref. 1.

For receiver ranges $\rho < 4l_y^2/\lambda$, where the internal wave inhomogeneities are fully correlated within the Fresnel width, from Eq. (74) of Ref. 1, we have

$$\begin{aligned}\int_0^\rho \mu_n(\rho_s)\mathrm{d}\rho_s &= \sum_m \rho\frac{l_x}{\xi_m}\frac{1}{|\xi_m|}[\langle|\Xi_h(m,n,0,0)|^2\rangle - |\langle\Xi_h(m,n,0,0)\rangle|^2],\end{aligned} \tag{28}$$

and for receiver ranges $\rho > 4l_y^2/\lambda$, where the Fresnel width exceeds the internal wave cross-range coherence length, from Eq. (90) of Ref. 1, we have

$$\int_0^\rho \mu_n(\rho_s)\mathrm{d}\rho_s = \sum_m 2\left(\frac{l_x}{\xi_m}\rho_s^{\mathrm{cor}} + A_c\sqrt{\frac{\rho}{2\pi\xi_m}}\left[\sin^{-1}\sqrt{1-\frac{\rho_s^{\mathrm{cor}}}{\rho}} - \sin^{-1}\sqrt{\frac{\rho_s^{\mathrm{cor}}}{\rho}}\right]\right)\frac{1}{|\xi_m|}[\langle|\Xi_h(m,n,0,0)|^2\rangle - |\langle\Xi_h(m,n,0,0)\rangle|^2], \tag{29}$$

where $\rho_s^{\mathrm{cor}} = \rho/2(1-\sqrt{1-4l_y^2/\lambda\rho})$. These equations show how the exponential coefficient of modal field variance couples energy in incident mode n to all scattered modes m after random multiple forward scattering through the waveguide.

The mean forward field of Eq. (23) is also called the coherent field, the magnitude square of which is proportional to the coherent intensity. The variance of the forward field in Eq. (27) provides a measure of the incoherent intensity. The total intensity of the forward field is the sum of the coherent and incoherent intensities. The coherent field tends to dominate at short ranges from the source and in slightly random media, while the incoherent field tends to dominate in highly random media. It should be noted that in a nonrandom waveguide $\mu_n = 0$ so that the variance of the forward field is zero, from Eq. (27). This is expected since the field is fully coherent in this case.

D. Modal attenuation from generalized waveguide extinction theorem

Attenuation or extinction of the forward field arises from scattering by inhomogeneities and intrinsic absorption in the medium. As mentioned in Secs. I and II C, the purely real scatter function of Eq. (13) can only account for dispersion due to scattering. In order to include attenuation in the mean forward field, we apply the waveguide extinction theorem.[3,4] The modal extinction cross section of an object, for incident mode n, is the ratio of the extinction $\mathcal{E}_n$ or power loss caused by the object to the incident intensity $I_{i,n}$,[3,4]

$$\sigma_n(x=0) = \frac{\mathcal{E}_n(x=0|\mathbf{r_0})}{I_{i,n}(z_h|\mathbf{r_0})\cdot\mathbf{i}_x}, \tag{30}$$

where $\mathbf{i}_x$ is the propagation direction. The notation $x=0$ means that the medium's intrinsic absorption is set to zero

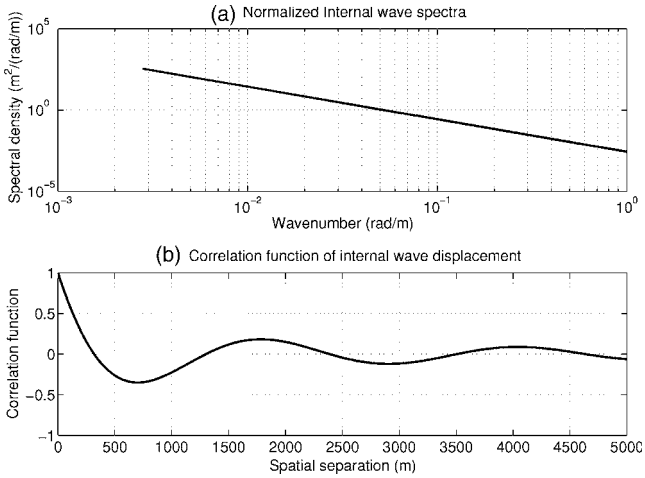

FIG. 2. (a) Normalized spectrum of internal wave field over an observation period of approximately 10 min with minimum wave number $\kappa_{\min}=0.028$ rad/m. The spectrum is computed using Eq. (22) with a κ^{-2} dependence at high frequencies. (b) Correlation function of the isotropic internal wave field with a coherence length of 100 m. The correlation function was obtained from the inverse Fourier transform of the internal wave spectrum plotted in (a).

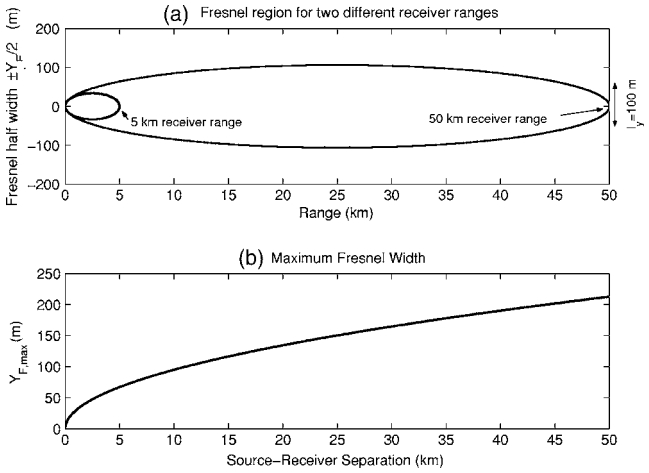

FIG. 3. (a) Fresnel half-width for receiver ranges $\rho=5$ km and $\rho=50$ km. The Fresnel width $Y_F(\rho,\rho_s)$ is approximately equal to $\sqrt{\lambda(\rho-\rho_s)\rho_s/\rho}$, where ρ is the source-receiver separation and ρ_s is the range from source to inhomogeneity. (b) The maximum Fresnel width $Y_{F,\max}=Y_F(\rho,\rho/2)=\sqrt{\lambda\rho}/2$ as a function of source-receiver separation ρ.

during the calculation, as described in Ref. 3, to properly determine the extinction cross section of a given scatterer.

In a waveguide with random internal wave inhomogeneities, the modal attenuation coefficient $\Im\{\nu_n\}$ can be be expressed in terms of the modal extinction cross section[3] $\sigma_n(x=0|h)$ of the inhomogeneities as

$$\Im\{\nu_n(\rho_s)\}=\frac{1}{2A_c(\rho_s)}\left\langle\frac{1}{d(z_h)}\sigma_n(x=0|h)|u_n(z_h)|^2\right\rangle, \tag{31}$$

from Eq. (60) of Ref. 1 and Eq. (20) of Ref. 3, where the expectation in Eq. (31) is taken over the height of the internal waves. Note that

$$A_c(\rho_s)=\begin{cases}A_{\mathrm{F}}, & l_y>Y_{\mathrm{F}}(\rho_s)\\ A_c, & l_y<Y_{\mathrm{F}}(\rho_s),\end{cases} \tag{32}$$

is dependent on the range location ρ_s of the inhomogeneity within the Fresnel width from source to receiver, where A_{F} is defined in Sec. II B 2.

For nonabsorbing objects, the extinction $\mathcal{E}_m$ caused by the object is equal to the total scattered power $W_{s,n}$. By placing the object within a closed control surface, we can calculate $W_{s,n}$ as the total scattered power flux through the surface. A general analytic expression for the total scattered power flux from an object centered at depth z_h within a closed cylindrical control surface with a radius of x and height spanning the entire waveguide depth for incident mode n is provided by Eq. (16) of Ref. 3. We assume that the internal wave elements remove power from the incident field by scattering only so that intrinsic absorption losses from the inhomogeneities are negligible. This is a valid assumption since the internal wave inhomogeneities do not lead to absorption other than that already present in the medium. For a characteristic internal wave inhomogeneity given height h, the total scattered power flux is

$$W_{s,n}(x|\mathbf{r_0},h)=\Re\left\{\frac{1}{\omega d^2(z_0)}\frac{|u_n(z_0)|^2}{|\xi_n|x_0}\sum_{m=1}^{\infty}\frac{\xi_m}{|\xi_m|}A_c^2(\rho_s)\times e^{-2\Im\{\xi_n x_0+\xi_m x\}}\int_0^{2\pi}|\Xi_h(m,n,\beta,0)|^2\,d\beta\right\}. \tag{33}$$

The x component of incident intensity from mode n on this inhomogeneity is

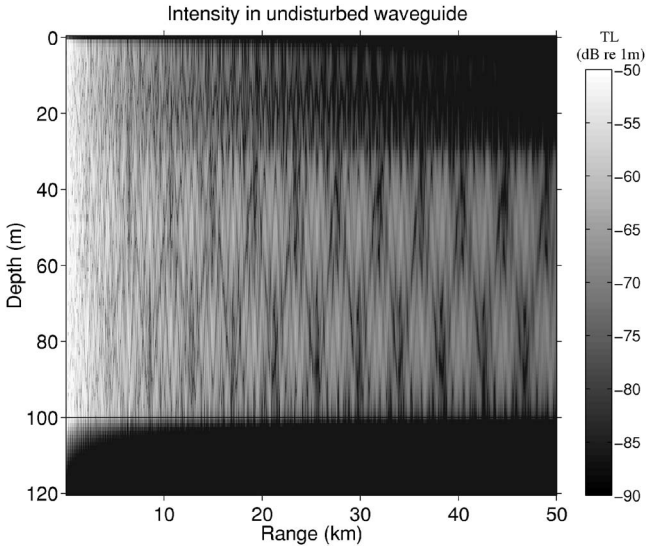

FIG. 4. Acoustic field intensity at 415 Hz as a function of range and depth in the mid-latitude Atlantic continental shelf waveguide of Fig. 1, when there are no internal waves present so that the waveguide is undisturbed. The boundary between the warm and cool water is at the depth of 30 m from the water surface in this static waveguide. The source is at 50 m depth with source level 0 dB *re* 1 μPa at 1 m. The acoustic intensity exhibits range- and depth-dependent variations due to coherent interference between waveguide modes.

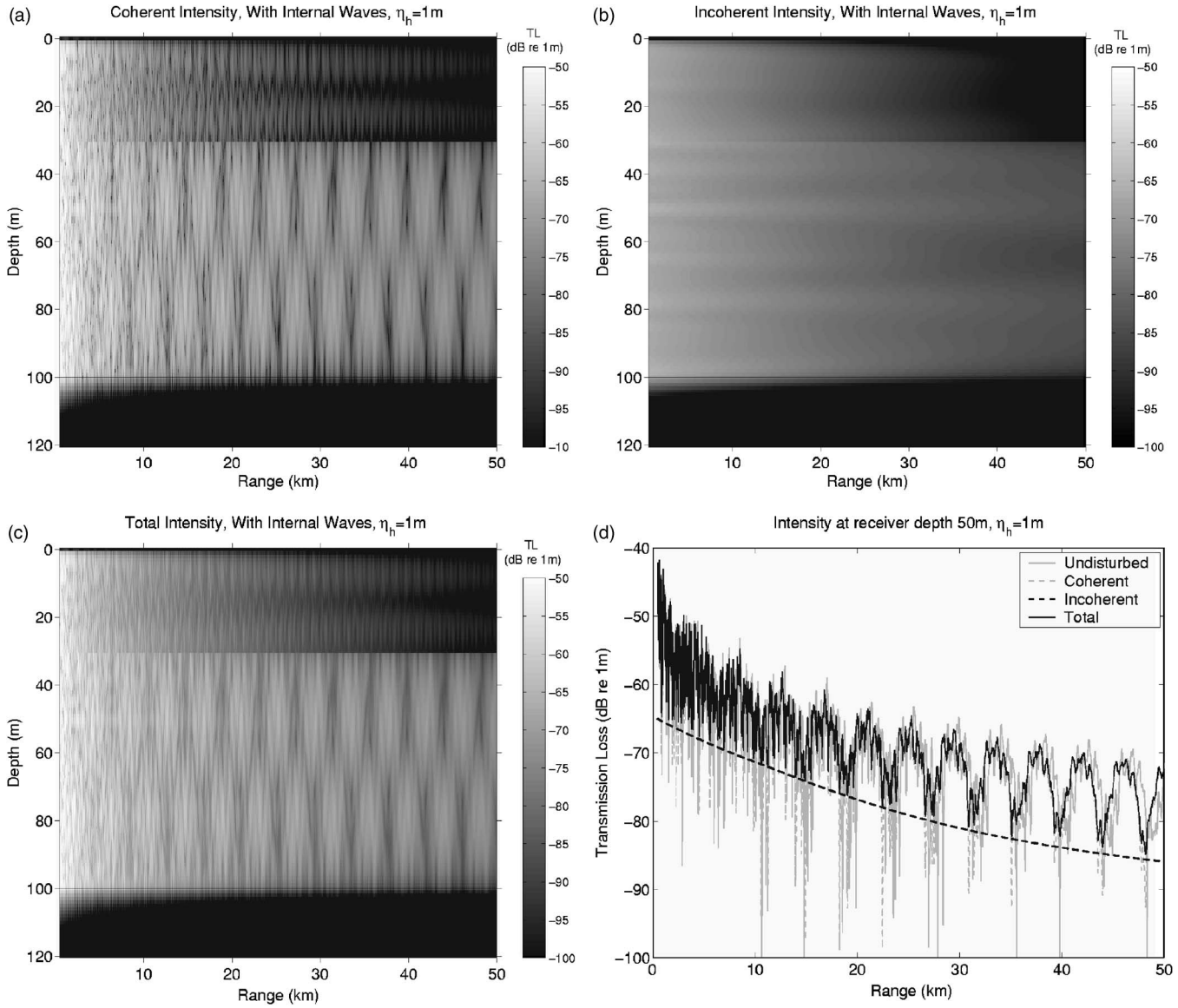

FIG. 5. Intensities of the (a) mean or coherent field, (b) variance or incoherent field, and (c) the total field at 415 Hz as functions of range and depth in the mid-latitude Atlantic continental shelf waveguide of Fig. 1 when there is a random internal wave field present in the waveguide. The internal wave disturbances have a height standard deviation of σ_h=1 m and coherence lengths of l_x=l_y=100 m. The source is at 50 m depth with source level 0 dB *re* 1 μPa at 1 m. This medium is only slightly random and the total intensity in (c) is dominated by the coherent intensity out to 50 km range and exhibits range- and depth-dependent variations due to coherent interference between waveguide modes, similar to the static waveguide example in Fig. 4. Figure 5(d) shows the acoustic intensity as a function of range at a single receiver depth of 50 m for the fields shown in (a)–(c). For a comparison, the acoustic intensity of the static waveguide is also plotted.

$$I_{i,n}(z_t|\mathbf{r_0})\cdot\mathbf{i}_x = \frac{2\pi}{\omega d^2(z_0)d(z_h)}\frac{1}{x_0}|u_n(z_0)|^2|u_n(z_h)|^2\frac{\Re\{\xi_n^*\}}{|\xi_n|} \times e^{-2\Im\{\xi_n\}x_0}, \tag{34}$$

from Eq. (19) of Ref. 3. Following Eq. (30), the modal extinction cross section of the internal wave inhomogeneity is found from dividing Eq. (33) by Eq. (34) and setting x=0,

$$\sigma_n(x=0|h) = \Re\left\{\frac{1}{2\pi}d(z_h)\frac{1}{|u_n(z_h)|^2}\sum_{m=1}^{\infty}\frac{\xi_m^*}{|\xi_m|\Re\{\xi_n^*\}}A_c^2(\rho_s) \times\int_0^{2\pi}|\Xi_h(m,n,\beta,0)|^2\,\mathrm{d}\beta\right\}. \tag{35}$$

The attenuation coefficient of mode n due to scattering in the random waveguide can then be found to be

$$\Im\{\nu_n(\rho_s)\} = \frac{1}{4\pi}A_c(\rho_s)\sum_{m=1}^{\infty}\Re\left\{\frac{\xi_m^*}{|\xi_m|\Re\{\xi_n^*\}}\int_0^{2\pi}\langle|\Xi_h(m,n,\beta,0)|^2\rangle\mathrm{d}\beta\right\}, \tag{36}$$

by substituting Eq. (35) into Eq. (31).

III. COMPUTING 2-D SPATIAL REALIZATIONS OF A RANDOM INTERNAL WAVE FIELD

To compare statistical moments of the forward field from the 3-D analytical formulation with Monte-Carlo simu-

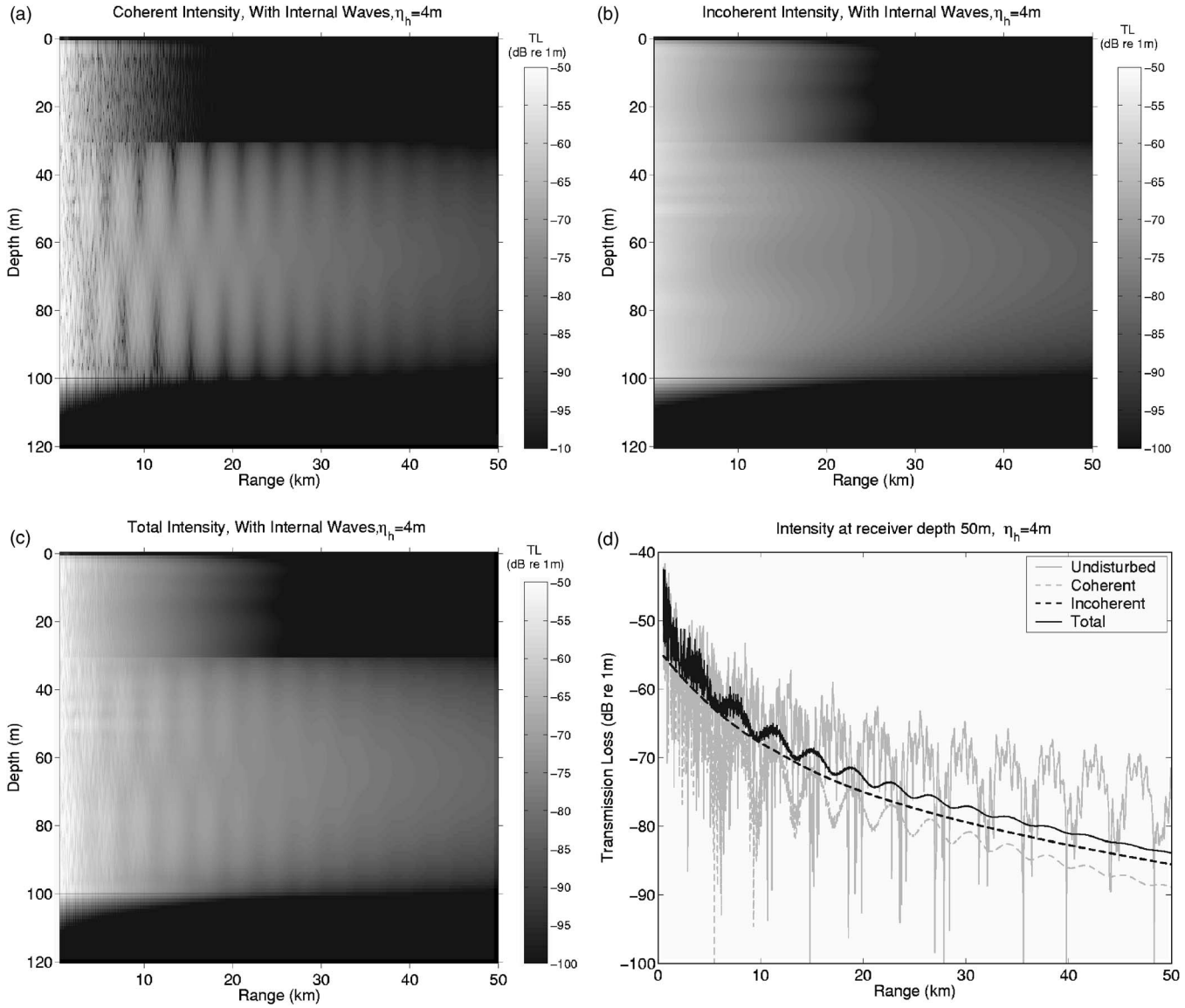

FIG. 6. Similar to Fig. 5, but for a waveguide with an internal wave height standard deviation of η_h=4 m. This medium is highly random and the total intensity in (c) is dominated by the variance or incoherent intensity beyond the 11 km range. The total acoustic intensity decays monotonically as a function of range at sufficiently long ranges since the field is now completely incoherent and the waveguide loses the coherent range- and depth-dependent variations due to modal interference.

lations based on the 2-D parabolic equation, we must compute spatial realizations of the internal wave height $h(x_t)$. We assume that the Gaussian random internal wave field $h(x_t)$ is a stationary random process that follows the correlation function shown in Fig. 2(b). The Fourier transform of internal wave height $h(x_t)$ over a finite spatial window is then

$$H(\kappa) = \int_{-L/2}^{L/2} h(x_t) e^{-i\kappa x_t} \, dx_t,$$

where $H(\kappa)$ is a zero-mean Gaussian random process due to its linear dependence on $h(x_t)$. According to Parseval's theorem,

$$\eta_h^2 \approx \frac{1}{L} \int_{L/2}^{L/2} \langle |h(x_t)|^2 \rangle dx_t = \frac{1}{L} \int \langle |H(\kappa)|^2 \rangle d\kappa, \tag{37}$$

while, from Eq. (6), $\eta_h^2 = C_{hh}(0)$, so that $\langle |H(\kappa)|^2 \rangle \approx L\mathcal{G}(\boldsymbol{\kappa})\kappa/2\pi$. As L becomes arbitrarily large, the delta-function correlation is achieved across the wave number domain,

$$\langle H(\kappa) H(\kappa') \rangle \approx \frac{\mathcal{G}(\boldsymbol{\kappa})\kappa}{2\pi} \delta(\kappa - \kappa'), \tag{38}$$

indicating that components of $H(\kappa)$ with wave number separations exceeding $2\pi/L$ are uncorrelated.

So, a random realization of the internal wave height $h(x_t)$ can be computed as the inverse Fourier transform of $H(\kappa)$ under the assumption that the $H(\kappa)$ are zero mean Gaussian random variables that are uncorrelated when sampled at wave number intervals of at least $2\pi/L$ and have variance $L\mathcal{G}(\boldsymbol{\kappa})\kappa/2\pi$.

IV. ILLUSTRATIVE EXAMPLES

Here we provide examples illustrating the dependence of acoustic field moments on internal wave parameters. We

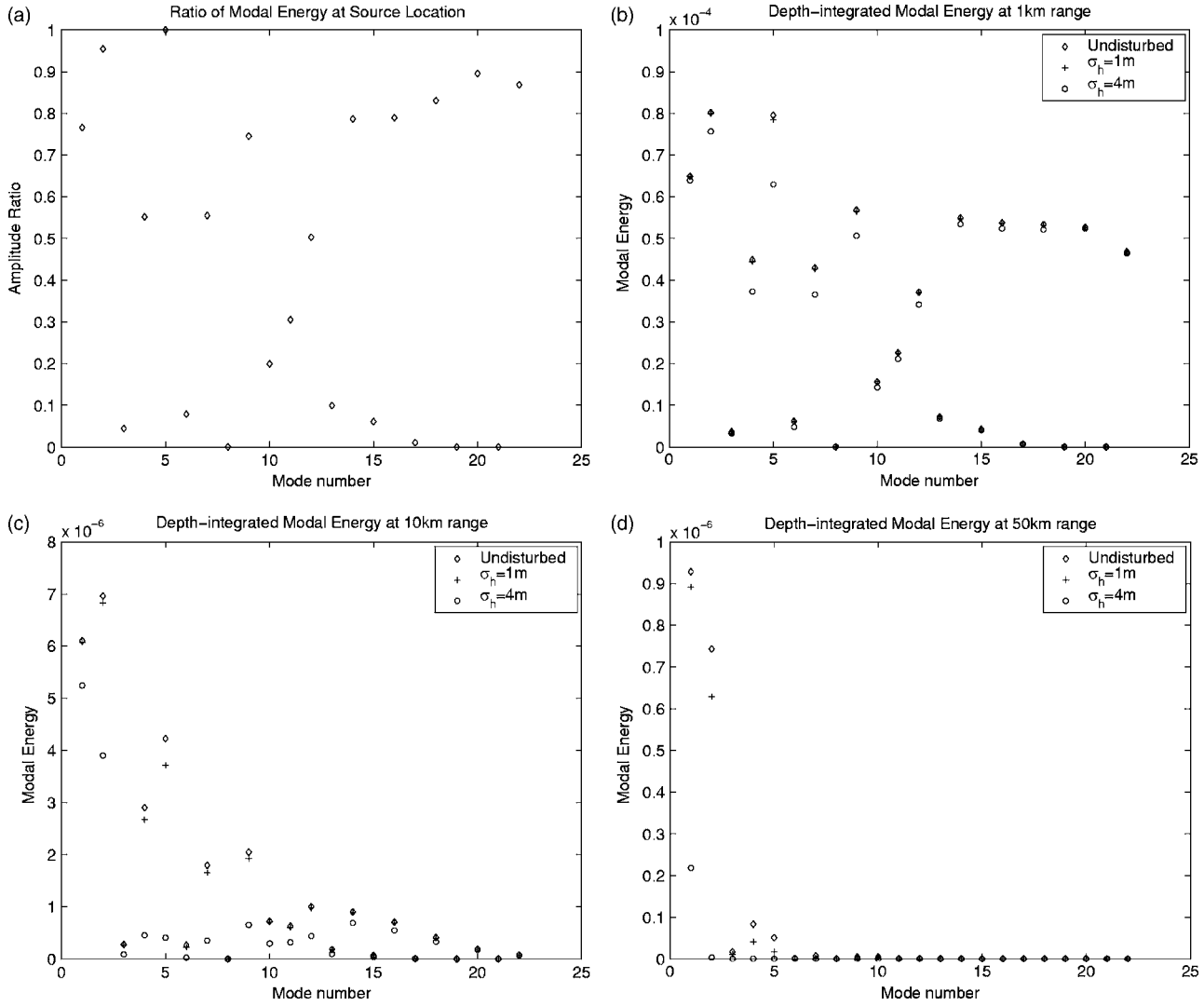

FIG. 7. Contributions of the waveguide modes to the depth-integrated total intensity of the forward field at (a) the source location, (b) 1 km, (c) 10 km, and (d) 50 km ranges from the source for a source strength of 0 dB *re* 1 μPa at 1 m. All values are absolute except those in (a), which are normalized by the maximum modal contribution.

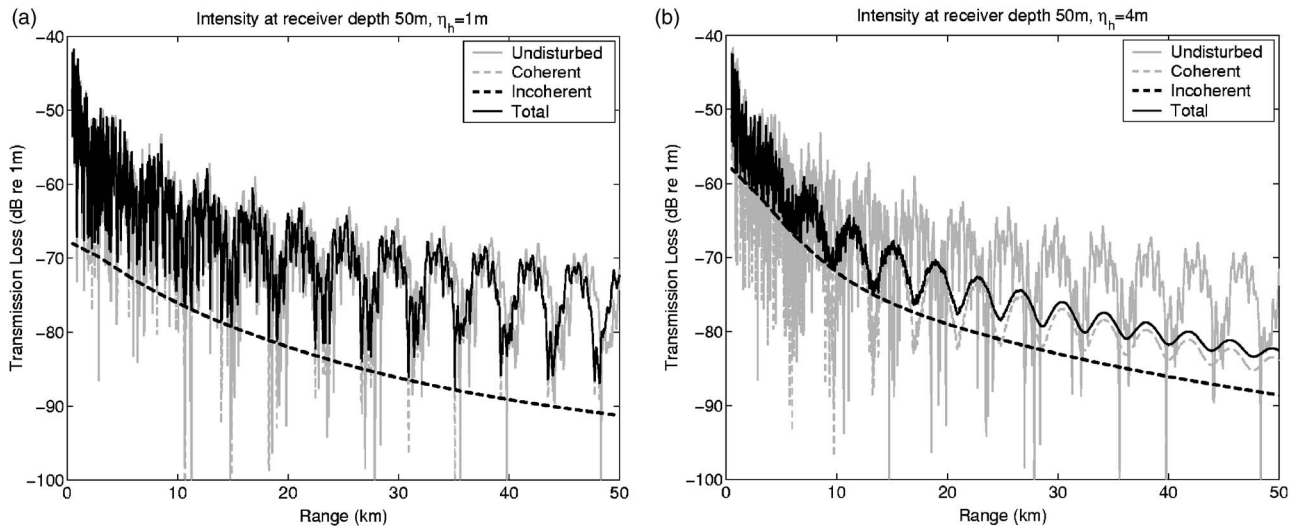

FIG. 8. Acoustic intensity at a single receiver depth of 50 m in the presence of an internal wave field with coherence lengths $l_x = l_y = 50$ m and height standard deviations of (a) $\eta_h = 1$ m and (b) $\eta_h = 4$ m.

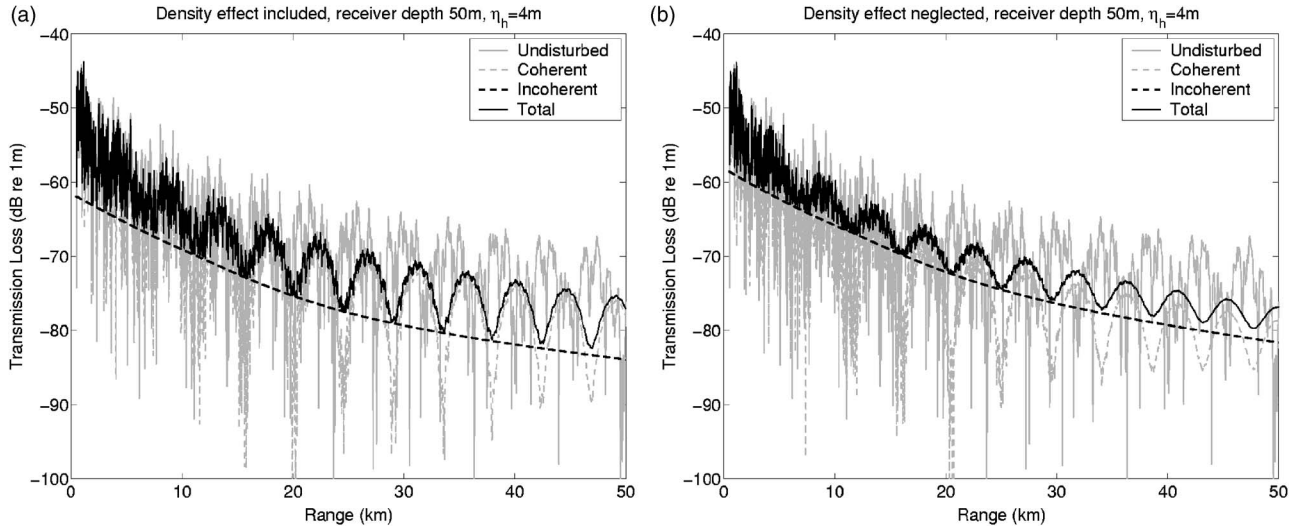

FIG. 9. Effect of (a) including and (b) neglecting internal wave density fluctuations on acoustic transmission in an Arctic waveguide with geometry described in Fig. 1. The internal wave field has coherence lengths of $l_x = l_y = 100$ m and a height standard deviation of $\eta_h = 4$ m. The acoustic intensity is plotted as a function of range for the source and receiver at 50 m depth.

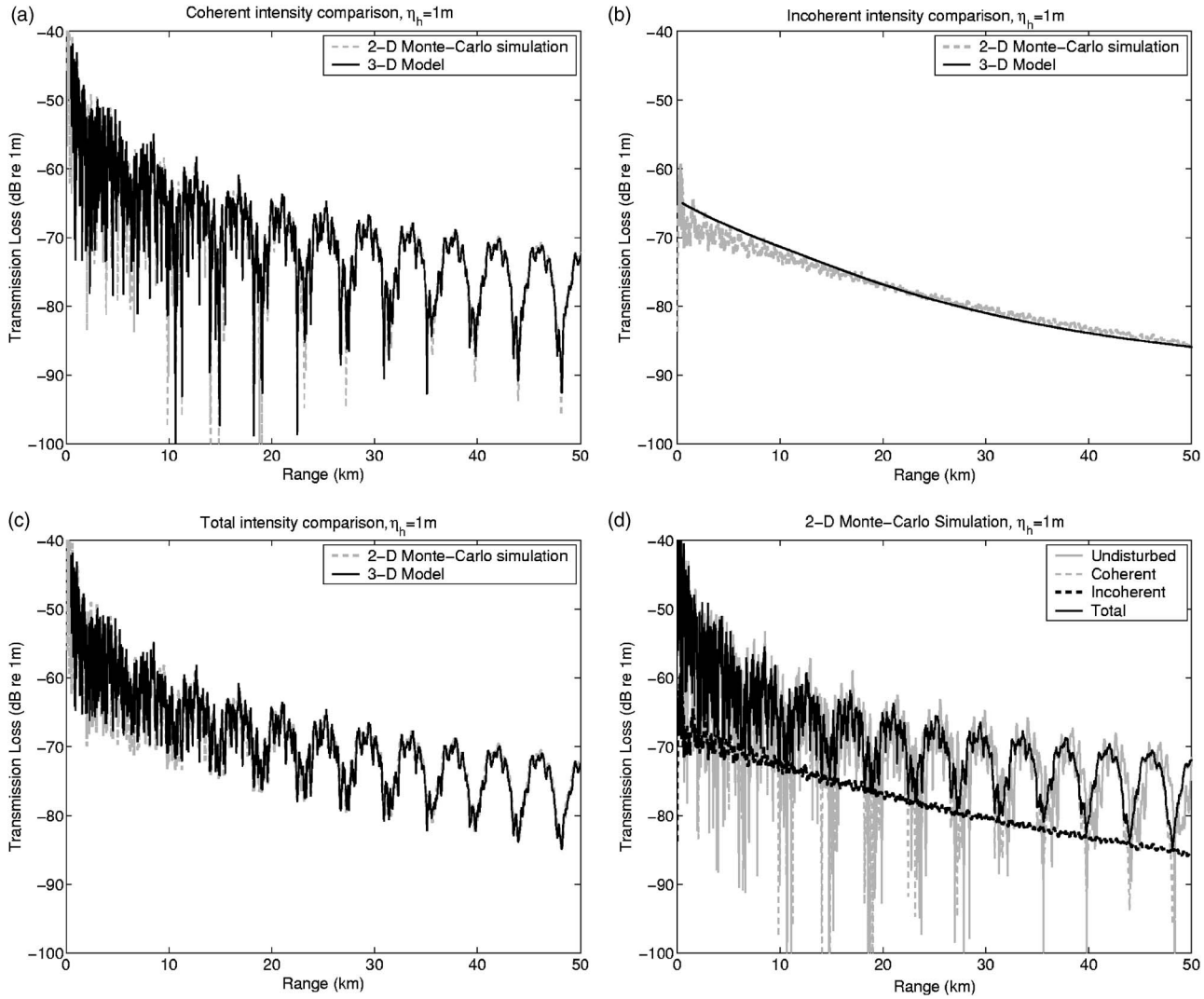

FIG. 10. Comparison of intensities from 2-D Monte-Carlo simulations and 3-D analytical model at the single receiver depth of 50 m in the presence of an internal wave field with height standard deviation of $\eta_h = 1$ m. A total of 1000 simulations were made using the parabolic equation to compute the 2-D Monte Carlo field statistics. (a) Coherent field comparison, (b) incoherent field comparison, (c) total field comparison, (d) only the 2-D Monte-Carlo simulated acoustic intensities of the coherent, incoherent, and total fields used in (a)–(c).

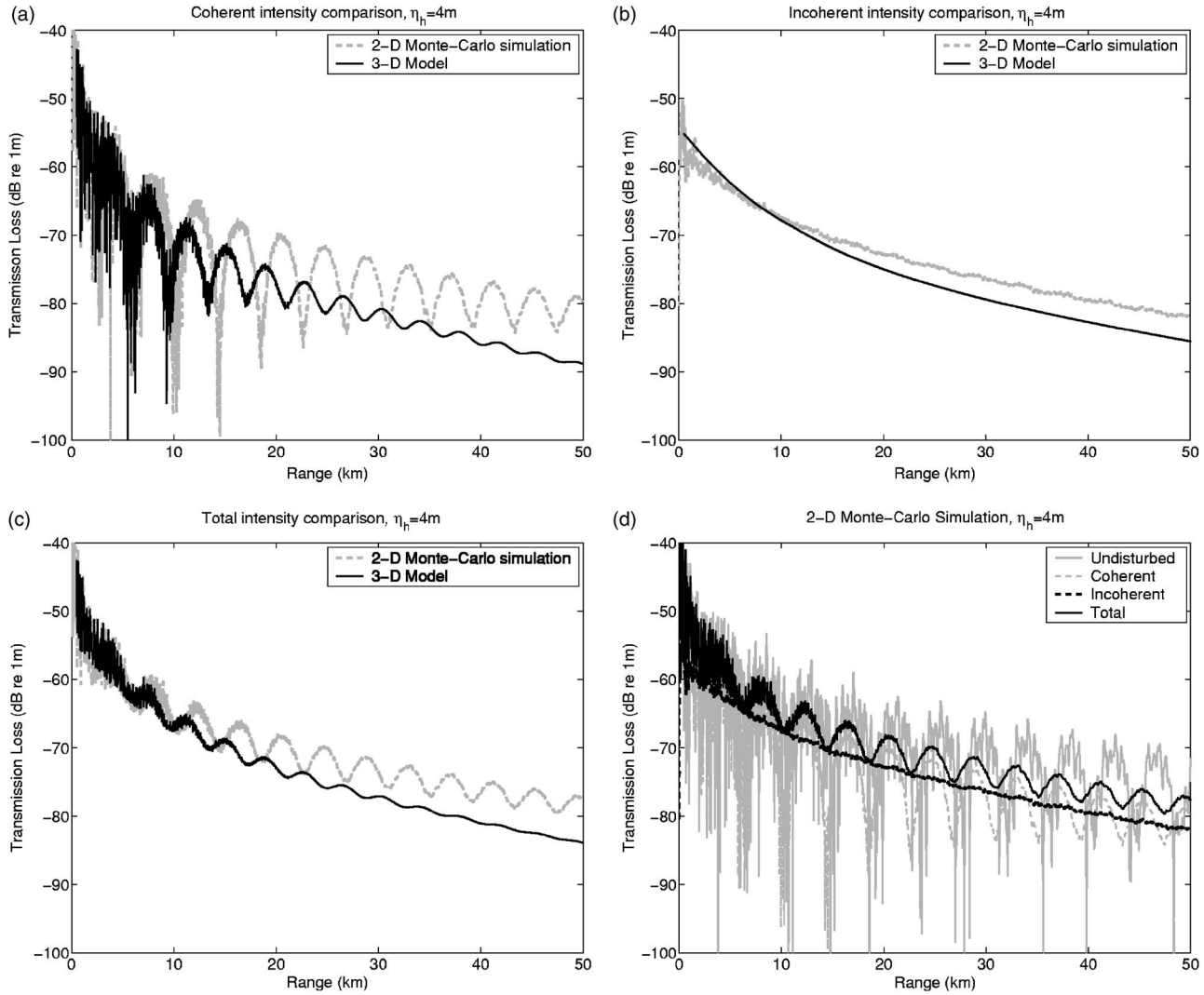

FIG. 11. Similar to Fig. 10, but for a waveguide with an internal wave height standard deviation of η_h=4 m.

study random and isotropic internal waves in typical continental shelf environments. In Sec. IV A, we investigate the effect of rms internal wave height and coherence length on acoustic transmission in a typical mid-latitude Atlantic continental shelf waveguide. In Sec. IV B, the coherent, incoherent, and total intensities of the forward acoustic field are compared when density fluctuations due to internal waves are first included and then neglected. We also compare our 3-D analytical model with 2-D Monte-Carlo simulations of the forward propagated acoustic field in Sec. IV C.

We examine the effect of internal waves on acoustic transmission over a measurement time period of approximately 10 min in our simulations. Over this time period, internal wave disturbances with wave numbers larger than $\kappa_{\min}$=0.028 rad/m will undergo spatial-temporal variation. The normalized power spectrum of the internal wave field is shown in Fig. 2(a) and the correlation function in Fig. 2(b). The corresponding coherence length of the isotropic internal waves is l_x=l_y=100 m from Fig. 2 and Eqs. (8), (9), and (10). The maximum Fresnel width $\sqrt{\lambda\rho/2}$ then exceeds the cross-range coherence length for source-receiver separations larger than 11 km, as shown in Fig. 3. These are the ranges

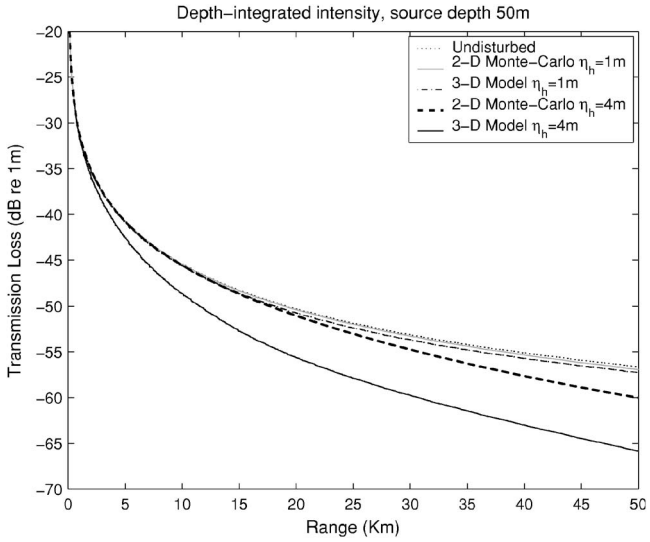

FIG. 12. Total depth-integrated intensities for the waveguide used in Fig. 4. The static case with no internal waves in the medium is compared to the 3-D analytical model and 2-D Monte-Carlo simulations with internal wave height standard deviations of η_h=1 m and η_h=4 m. The attenuation or power loss due to scattering is most significant in the 3-D analytical model for the highly random waveguide.

where 3-D scattering effects can become pronounced when internal wave displacements exceed the acoustic wavelength.

A. Mid-latitude Atlantic continental shelf environment

Here, a water column of $H=100$ m depth is used to simulate the geometry of a typical continental shelf environment, as shown in Fig. 1. The water column is comprised of a warm upper layer with density $d_1=1024$ kg/m^3 and sound speed $c_1=1520$ m/s overlying a cool lower layer with density $d_2=1025$ kg/m^3 and sound speed $c_2=1500$ m/s. The bottom sediment half-space is composed of sand with density $d_b=1.9$ g/cm^3 and sound speed $c_b=1700$ m/s. The attenuations in the water column and bottom are $\alpha=6\times10^{-5}$ dB/λ and $\alpha_b=0.8$ dB/λ, respectively. The 3-D internal wave field is assumed to propagate along the boundary between the two layers at a depth of $D=30$ m from the surface. The receiver and source with frequency 415 Hz and source level of 0 dB *re* 1 μPa at 1 m are both located at 50 m depth in the water column.

We consider two scenarios. In the first scenario, the internal wave disturbances have a height standard deviation of $\eta_h=1$ m that is smaller than the acoustic wavelength of λ $=3.6$ m. For the ranges considered, we find the acoustic field to be slightly random. The internal wave spectrum has an amplitude of approximately 2 m^2/cph at $\kappa_{\min}$ for this example. In the second scenario, the internal wave disturbances have a height standard deviation of $\eta_h=4$ m, which is slightly larger than the acoustic wavelength. We find that the acoustic field becomes highly random within a few kilometers of the source. The internal wave spectrum has an amplitude of approximately 30 m^2/cph at $\kappa_{\min}$ in this case. The internal wave correlation length and height standard deviations modeled here are typical of those measured on the Strataform area of the New Jersey continental shelf. For instance, they would correspond to the disturbances shown as Segment C of Fig. 24 in Ref. 7.

The acoustic field intensity is plotted as a function of range and depth in Fig. 4 for the shallow water waveguide of Fig. 1 when there are no internal waves present in the medium. The waveguide is static and undisturbed by inhomogeneities in this case. The forward acoustic field is then fully coherent, since the variance in the forward field is zero everywhere in the medium. The acoustic intensity exhibits a range- and depth-dependent structure arising from coherent interference between the waveguide modes. Figure 5 shows the coherent, incoherent, and expected total intensity for the slightly random waveguide. In this case, the incoherent intensity is small compared to the coherent intensity even at long ranges up to 50 km. The total field still maintains the range- and depth-dependent structure due to modal interference, but shows the effect of some moderate dispersion and attenuation. The situation changes, however, in the highly random waveguide, as shown in Fig. 6. The coherent intensity decays rapidly as a function of range from the source due to severe attenuation arising from internal wave scattering. The incoherent component dominates the expected total intensity beyond the 11 km range, where 3-D scattering begins to take effect. The expected total intensity eventually decays monotonically with range and no longer exhibits a significant coherent modal interference structure in range and depth beyond roughly 30 km in range.

The relative contributions of the waveguide modes to the depth-integrated total intensity of the forward field at the source location and at 1, 10, and 50 km range from the source are shown in Fig. 7. There it can be seen that the highly random waveguide redistributes modal energies far more than the nonrandom waveguide and also has much less energy across the modal spectrum.

We next investigate the dependence of the forward field moments on the coherence lengths of the internal wave disturbances by letting them decrease to $l_x=l_y=50$ m. Figures 8(a) and 8(b) show the coherent, incoherent, and total acoustic intensities for internal wave height standard deviations of $\eta_h=1$ m and $\eta_h=4$ m, respectively. Comparing the coherent field in Figs. 8(a) and 8(b) with Figs. 5(d) and 6(d), we find that attenuation due to scattering increases with increasing coherence length, especially in the highly random waveguide. This can be explained by noting that in Eq. (36) the attenuation coefficient is linearly related to the coherence area since the second moment of scatter function density is effectively independent of coherence area in the forward azimuth. The larger attenuation from multiple scattering leads to lower coherent intensity. The level of incoherent intensity, on the other hand, increases with increasing coherence area in the highly random waveguide. This is expected, since in the limiting case where the cross-range coherence length exceeds the Fresnel width, incoherent intensity arises from a more multiplicative process of transmission through single scatter shells decorrelated solely in range as in a 2-D multiple scattering scenario.[37,38]

B. Effect of internal wave density fluctuations on acoustic transmission in an Arctic environment

Internal waves cause not only sound speed, but also density fluctuations in the water column that can sometimes affect acoustic transmission statistics. Density effects are expected to be pronounced in deep estuaries such as Norwegian Fjords, where "fresh river water tends to move seaward above the heavier salt water[29]," before sufficient tidal motions occur to cause mixing,[29] and in the Arctic seas, where cold fresh water near the melting temperature of ice flows above warm and salty seawater.[36]

Here we give an example of acoustic propagation though a 3-D linear internal wave field in an Arctic sea with 100 m water depth, as illustrated in Fig. 1. The interface between the cold fresh water above with density $d_1=1022$ kg/m^3 and sound speed $c_1=1433$ m/s and the warm salty water below with density $d_2=1028$ kg/m^3 and sound speed $c_2=1443$ m/s is also assumed to be at 30 m depth from the sea surface.[36] In Fig. 9, we determine the effect of internal wave density fluctuations on the forward acoustic field by including and then neglecting them in our calculations. Significant differences occur between these two cases for both the coherent and incoherent field components. Attenuation due to scattering is reduced when density fluctuations are included. This is because scattering from density and compressibility inhomogeneities are exactly out of phase

in the forward direction, as can be seen by substituting sound speeds and densities for the two layers of the water column into Γ_κ and Γ_d in Eq. (18). Internal wave density fluctuations should then not be neglected in estimating acoustic transmission statistics in certain environments.

C. Comparison of 3-D analytic model with 2-D Monte-Carlo simulations

Comparisons of the coherent, incoherent, and total acoustic field intensity determined by our 3-D analytic model and 2-D Monte-Carlo simulations using the parabolic equation for a slightly random waveguide with $\eta_h = 1$ m are illustrated in Figs. 10(a), 10(b), and 10(c). The coherent, incoherent, and total intensities calculated with the 3-D and 2-D approaches match very well out to the 50 km ranges shown. Both the 3-D and 2-D simulations agree on the moderate dispersion, attenuation, and low variance or incoherent intensity found at the longer ranges shown. This is a consequence of the weak scattering found for rms internal wave displacements, small compared to the acoustic wavelength. The situation changes, however, in a highly random waveguide, where rms internal wave displacements exceed the acoustic wavelength, with $\eta_h = 4$ m. As shown in Figs. 11(a), 11(b), and 11(c), the coherent and incoherent fields determined by the two approaches show a reasonable match within 11 km, where the cross-range coherence is larger than the Fresnel width. This is the range within which the 2-D simulations are expected to be valid. Beyond 11 km range, the 2-D Monte-Carlo simulations of coherent and incoherent intensities are far less attenuated than those of the 3-D model and the 2-D coherent intensities are far less dispersed. This is because the 2-D parabolic equation cannot account for scattering of acoustic energy out of the forward direction and subsequent loss of coherence incurred by random cross-range variations in the 3-D medium. Figures 10(d) and 11(d) show 2-D Monte-Carlo simulations of the coherent, incoherent and total field for the slightly and highly random waveguides for comparison with the 3-D model examples of Figs. 5(d) and Fig. 6(d).

The expected values of depth-integrated total intensity for our 3-D model and 2-D Monte-Carlo simulations are compared in Fig. 12. They decay with range as a result of spreading, intrinsic absorption and the accumulated effect of multiple forward scattering through internal wave inhomogeneities in the medium. In the slightly random waveguide, the curves for the 3-D and 2-D models show close agreement with each other and with the curve for the undisturbed waveguide, as expected, since scattering is weak. In the highly random waveguide, the 3-D model shows far greater power loss than the 2-D Monte-Carlo simulations. This is because the 2-D model cannot account for the out-of-plane scattering that must occur when the Fresnel width exceeds the cross-range coherence length of the internal waves.

V. CONCLUSION

Statistical moments of the acoustic field forward propagated through an ocean waveguide with random internal waves are modeled with a normal mode formulation that accounts for 3-D multiple forward scattering through medium inhomogeneities. The formulation analytically describes the accumulated effects of *multiple forward scattering*. These redistribute both coherent and incoherent modal energy, including attenuation and dispersion. Calculations for typical continental shelf environments show that the acoustic field becomes effectively incoherent at typical operational ranges when the rms internal wave height is on the order of the acoustic wavelength. It is found that two-dimensional models for the mean and variance of the acoustic field propagated through a 3-D random internal wave field then become inaccurate when the Fresnel width approaches and exceeds the cross-range coherence length of the internal wave field. Density fluctuations caused by internal waves may have a non-negligible effect on acoustic transmission in certain continental shelf environments, such as in Arctic seas.

[1] P. Ratilal and N. C. Makris, "Mean and covariance of the forward field propagated through a stratified ocean waveguide with three-dimensional random inhomogeneities," submitted to J. Acoust. Soc. Am.

[2] P. M. Morse and K. U. Ingard, *Theoretical Acoustics* (Princeton University Press, Princeton, NJ, 1986).

[3] P. Ratilal and N. C. Makris, "Extinction theorem for object scattering in a stratified medium," J. Acoust. Soc. Am. **110**, 2924–2945 (2001).

[4] P. Ratilal, "Remote sensing of submerged objects and geomorphology in continental shelf waters with acoustic waveguide scattering," Ph.D thesis, Massachusetts Institute of Technology, 2002.

[5] J. Colosi, R. Beardsley, J. Lynch, G. Gawarkiewicz, C. Chiu, and A. Scotti, "Observations of nonlinear internal waves on the outer New England continental shelf during the summer Shelfbreak Primer study," J. Geophys. Res. **106**, 9587–9601 (2001).

[6] J. Lynch, G. Jin, R. Pawlowicz, D. Ray, A. Plueddeman, C. Chiu, J. Miller, R. Bourke, A. Parsons, and R. Muench, "Acoustic travel-time perturbations due to shallow-water internal waves and internal tides in the Barents Sea Polar Front: Theory and experiment," J. Acoust. Soc. Am. **99**, 803–821 (1996).

[7] J. R. Apel, M. Badiey, C.-S. Chiu, S. Finette, R. Headrick, J. Kemp, J. F. Lynch, A. Newhall, M. H. Orr, B. H. Pasewark, D. Tielbuerger, A. Turgut, K. Heydt, and S. Wolf, "An overview of the 1995 SWARM shallow-water internal wave acoustic scattering experiment," IEEE J. Ocean. Eng. **22**, 465-500 (1997).

[8] N. C. Makris, "The effect of saturated transmission scintillation on ocean acoustic intensity measurements," J. Acoust. Soc. Am. **100**, 769-783 (1996).

[9] I. Dyer, "Statistics of sound propagation in the ocean," J. Acoust. Soc. Am. **47**, 337–345 (1970)

[10] W. A. Kuperman and F. Ingenito, "Attenuation of the Coherent Component of Sound Propagation in Shallow Water with Rough Boundaries," J. Acoust. Soc. Am. **61**, 1178-1187 (1977).

[11] W. A. Kuperman and H. Schmidt, "Rough surface elastic wave scattering in a horizontally stratified ocean," J. Acoust. Soc. Am. **79**, 1767-1777 (1986).

[12] W. A. Kuperman and H. Schmidt, "Self-consistent perturbation approach to rough surface scattering in stratified elastic media," J. Acoust. Soc. Am. **86**, 1511-1522 (1989).

[13] B. H. Tracey and H. Schmidt, "Seismo-acoustic field statistic in shallow water," IEEE J. Ocean. Eng. **22**, 317-331 (1997).

[14] G. R. Sutton and J. J. McCoy, "Scattering of acoustics signals by inhomogeneities in a waveguide—a single scatter treatment," J. Acoust. Soc. Am. **60**, 833-839 (1976).

[15] D. B. Creamer, "Scintillating shallow water waveguides," J. Acoust. Soc. Am. **99**, 2825-2838 (1996).

[16] L. B. Dozier and F. D. Tappert, "Statistics of normal mode amplitudes in a random ocean. I. Theory," J. Acoust. Soc. Am. **63**, 353-365 (1978).

[17] T. Duda and J. Preisig, "A modeling study of acoustic propagation through moving shallow water solitary wave packets," IEEE J. Ocean. Eng. **24**, 16–32 (1999).

[18] D. Tilbürger, S. Finette, and S. Wolf, "Acoustic propagation through an internal wave field in a shallow water waveguide," J. Acoust. Soc. Am. **101**, 789-807 (1997).

[19]C. Penland, "Acoustic normal mode propagation through a three-dimensional internal wave field," J. Acoust. Soc. Am. **78** 1356-1365 (1985).
[20]P. Ratilal, I. Bersatos, T. Chen, M. Zanolin, and N. C. Makris, "Optimal passive source localization in a fluctuating ocean waveguide based on an analytic model for the mean field and covariance," J. Acoust. Soc. Am. **115**, 2473 (2004).
[21]N. C. Makris, P. Ratilal, M. Zanolin, and I. Bersatos, "Obtaining optimal time-delay, source localization and tracking estimates in free space and in an ocean waveguide," J. Acoust. Soc. Am. **116**, 2606 (2004).
[22]D. T. Symonds, P. Ratilal, N. C. Makris, and R. W. Nero "Inferring fish school distributions from long range acoustic images: Main acoustic clutter experiment 2003," J. Acoust. Soc. Am. **115**, 2618 (2004).
[23]P. Ratilal, D. T. Symonds, N. C. Makris, and R. W. Nero, "Fish population dynamics revealed by instantaneous continental-shelf scale acoustic imaging," J. Acoust. Soc. Am. **117**, 2382 (2005).
[24]M. Zanolin, I. Ingram, A. Thode, and N. C. Makris, "Asymptotic accuracy of geoacoustic inversions," J. Acoust. Soc. Am. **116**, 2031–2042 (2004).
[25]P. Ratilal, T. Chen, and N. C. Makris, "Estimating internal wave statistics from underwater acoustic transmission scintillation measurements on the New Jersey shelf with a 3-D stochastic model," J. Acoust. Soc. Am. **116**, 2506 (2004).
[26]L. M. Brekhovskikh and Y. Lysanov, *Fundamentals of Ocean Acoustics* (Springer-Verlag, New York, 1991).
[27]P. Hursky, M. B. Porter, B. D. Cornuelle, W. S. Hodgkiss, and W. A. Kuperman, "Adjoint modeling for acoustic inversion," J. Acoust. Soc. Am. **115**, 607-619 (2004).
[28]P. Ratilal, Y. Lai, D. T. Symonds, L. A. Ruhlmann, J. Goff, C. W. Holland, J. R. Preston, E. K. Scheer, M. T. Garr, and N. C. Makris, "Long range acoustic imaging in Continental Shelf Environment: The Acoustic Clutter reconnaisance Experiment 2001," J. Acoust. Soc. Am. **117**, 1977-1998 (2005). (Appendix A).
[29]J. Lighthill, *Waves in Fluids* (Cambridge University Press, Cambridge, 1978).
[30]A. E. Gill, *Atmosphere-Ocean Dynamics* (Academic Press, San Diego, 1082).
[31]W. A. Kuperman and J. F. Lynch, "Shallow-water acoustics," Phys. Today, **11**, 55–61 (2004).
[32]N. C. Makris, F. Ingenito, and W. A. Kuperman, "Detection of a submerged object insonified by surface noise in an ocean waveguide," J. Acoust. Soc. Am. **96**, 1703-1724 (1994).
[33]J. R. Apel, J. R. Holbrook, A. K. Liu, and J. J. Tsai, "The Sulu Sea Internal Soliton Experiment," J. Phys. Oceanogr. **15**, 1625-1651 (1985).
[34]L. A. Ostrovsky and Y. A. Stepanyants, "Do internal solitons exist in the ocean?," Rev. Geophys. **3**, 293-310 (1989).
[35]L. Mandel and E. Wolf, *Optical Coherence and Quantum Optics* (Cambridge University Press, Cambridge, 1995).
[36]N. C. Makris, "Environmental correlates of arctic ice edge noise," MIT Ph.D. thesis, 1991.
[37]B. R. Frieden, *Probability, Statistical Optics, and Data Testing* (Springer-Verlag, Berlin, (1936).
[38]J. W. Strobehn, in *Laser Beam Propagation in the Atmosphere* (Springer-Verlag, Germany, 1978).